

Scenario generation for market risk models using generative neural networks

Solveig Flaig^{*†}, Gero Junike[‡]

01.03.2022

Abstract

In this research, we show how to expand existing approaches of using generative adversarial networks (GANs) as economic scenario generators (ESG) to a whole internal model - with enough risk factors to model the full band-width of investments for an insurance company and for a one year time horizon as required in Solvency 2. For validation of this approach as well as for optimization of GAN architecture, we provide a consistent, data-driven framework using existing evaluation measures based on nearest neighbor distances and a newly developed measure for the detection of the memorizing effect. Finally, we demonstrate that the results of a GAN-based ESG are similar to regulatory approved internal models in Europe. Therefore, GAN-based models can be seen as an assumption-free data-driven alternative way of market risk modeling.

JEL classification C14, C45, C63, G22

Keywords Generative Adversarial Networks, Economic Scenario Generators, nearest neighbor distance, market risk modeling, Solvency 2

1 Introduction

The generation of realistic scenarios how the financial markets could behave in the future is one key component of internal market risk models used by insurance companies for Solvency 2 purposes. Currently, these are generated using economic scenario generators (ESGs) which are mainly based on financial mathematical models, see Bennemann [2011] and Pfeifer and Ragulina [2018]. These ESGs need strong assumptions on the behavior of the risk factors and their dependencies, are time-consuming to calibrate and it is difficult in this framework to model complex dependencies.

An alternative method for scenario generation can be a special type of neural networks called generative adversarial networks (GANs), invented by Goodfellow et al. [2014]. This network architecture consists of two neural networks which has gained a lot of attention due to its ability to generate real-looking pictures, see Aggarwal et al. [2021].

As financial data, at least for liquid instruments, is consistently available, GANs are used in various fields of finance, including market prediction, tuning of trading models, portfolio management and optimization, synthetic data generation and diverse types of fraud detection, see Eckerli and Osterrieder [2021]. Henry-Labordere [2019], Lezmi et al. [2020], Fu et al. [2019], Wiese et al. [2019], Ni et al. [2020] and Wiese et al. [2020] have already used GANs for scenario generation in the financial sector. The focus of their research was the generation of financial time series for a limited number of risk factors (up to 6) or a single asset class. To the best of our knowledge, there is no research performing a full value-at-risk calculation for an insurance portfolio based on GAN generated scenarios.

^{*}Corresponding author. Deutsche Rückversicherung AG, Kapitalanlage / Market risk management, Hansaallee 177, 40549 Düsseldorf, Germany. E-Mail: solveig.flraig@deutscherueck.de.

[†]Carl von Ossietzky Universität, Institut für Mathematik, 26111 Oldenburg, Germany.

[‡]Carl von Ossietzky Universität, Institut für Mathematik, 26111 Oldenburg, Germany. E-Mail: gero.junike@uol.de.

So far, the validation of the suitability of the GAN generated scenarios is mainly carried out visually or with a few statistic parameters, e.g. in Wiese et al. [2019], Ni et al. [2020] and Wiese et al. [2020]. However, a data-driven assessment of the GAN performance is desirable from two points of view: to validate the model to fulfill the requirements of Solvency 2 and to optimize the hyperparameters of the GAN and its architecture. In particular, measures based on nearest neighbor distances, as studied by Weiss [1960], Bickel and Breiman [1983], Schilling [1986], Henze [1988], Mondal et al. [2015] and Ebner et al. [2018] seem suitable.

In this research we

- expand the scenario generation by a GAN to a complete risk calculation serving for Solvency 2 purposes in insurance companies,
- provide a consistent, assumption-free framework for the evaluation of the scenario generation and the dependencies between risk factors,
- develop a new analytic measure for the detection of the memorizing effect
- and compare the results of a GAN-based ESG to the classical ESG approach implemented in regulatory approved market risk models in Europe.

The paper is structured as follows: In Section 2, we provide some background both on market risk calculation under Solvency 2 and on GANs. We explain how GANs can be employed as ESGs and the advantages and disadvantages of this approach. Section 3 recalls some measures from literature and presents a new measure to evaluate GAN generated scenarios. Additionally, we present a framework how to combine these measures for hyperparameter and architecture optimization. EIOPA (European Insurance and Occupational Pensions Authority) annually conducts a benchmarking exercise for approved market risk models in Europe, called MCRCs. This study together with a comparison of the results of a GAN-based ESG to the results in the study can be found in Section 4. Section 5 concludes.

2 Background

Before we present our work, we give a short introduction to the two main topics involved: economic scenario generators (ESG) and their usage for market risk calculation under Solvency 2 and generative adversarial networks (GANs).

2.1 Market risk calculation under Solvency 2

In 2016, a new regulation for insurance companies in Europe was introduced: Solvency 2. One central requirement is the calculation of the solvency capital requirement, called SCR. The SCR represents the risk of the insurer, see e.g. Gründl et al. [2019, Chapter 4]. The eligible capital of an insurance company is then compared with the SCR to determine whether the eligible capital is sufficient to cover the risks taken by the insurance company.

The solvency capital requirement equals the Value-at-Risk (VaR) at a 99.5%-level for a time horizon of 1 year, see Bennemann [2011, Chapter 2.3]. A mathematical definition of the VaR and a derivation of its usage in this context can be found in Denuit et al. [2006, p. 69].

The risk of an insurer can be divided into different modules: market risk, health underwriting risk, counterparty default risk, life underwriting risk, non-life underwriting risk and operational risk. The modules themselves consist of sub-modules, see EIOPA [2014]. Market risk, e.g. consists of the six submodules: interest rate, equity, property, spread, currency and concentration risk.

The SCR can be calculated using either the standard model or an internal model. For the standard model, the regulatory framework sets specific rules for the calculation for each risk encountered by the insurance company, defined in European Commission [2015]. Each internal model has to cover the same types of risks as the standard model and must be approved by local supervisors to ensure accordance with the principles of Solvency 2.

In this work, we will focus on the calculation of the market risk of a non-life insurer. However, the methods presented here can be applied for other risks, too. The reason for selecting market risk here is threefold:

- the underlying data in the financial market is publicly available and equal for all insurers,
- market risk forms a major part of the SCR of an insurance company (EIOPA [2018, p. 26] states that market risk accounts for 60% of the net solvency capital requirement before diversification benefits) and
- a comprehensive benchmark exercise, called “market and credit risk comparison study” MCRCS conducted by EIOPA is available for comparison of the results.

Current internal models for market risk often use Monte-Carlo simulation techniques to derive the risk of the (sub)modules and then use correlations or copulas for aggregation, see Bennemann [2011, p. 189] and Pfeifer and Ragulina [2018]. The basis of the Monte-Carlo simulation is a scenario generation performed by an “economic scenario generator” ESG. This ESG implements financial-mathematical models for all relevant risk factors (e.g. interest rate, equity) and their dependencies. Under those scenarios, the investment and liabilities portfolio of the insurer is evaluated and the risk is given by the 0.5%-percentile of the loss in these scenarios.

2.2 Generative adversarial networks

Generative adversarial networks, called GANs, are an architecture consisting of two neural networks which are used to play a minimax-game. In 2014, GANs were introduced by Goodfellow et al. [2014] and have gained a lot of attention afterwards because of their promising results especially in image generation. A good introduction to GANs can be found in Goodfellow et al. [2014], Goodfellow [2016] and Chollet [2018]. According to Motwani and Parmar [2020] and Li et al. [2020], GANs are one of the dominant methods for the generation of realistic and diverse examples in the domains of computer vision, image generation, image style transfer, text-to-image-translations, time-series synthesis, natural language processing, etc.

Other popular methods for the generation of data based on empirical observations are variational autoencoders and fully visible belief networks, see Goodfellow [2016, p. 14].

Technically, a GAN consists of two neural networks, named *generator* and *discriminator*. The discriminator network is trained to distinguish real data points from “fake” data points and assigns every given data point a probability that this data point is real. The input to the generator network is random noise coming from a so called *latent space*. The generator is trained to produce data points that look like real data points and would be classified by the discriminator as being real with a high probability. Figure 2.1, taken from Chen et al. [2018, p. 2], illustrates the general architecture of a GANs training procedure:

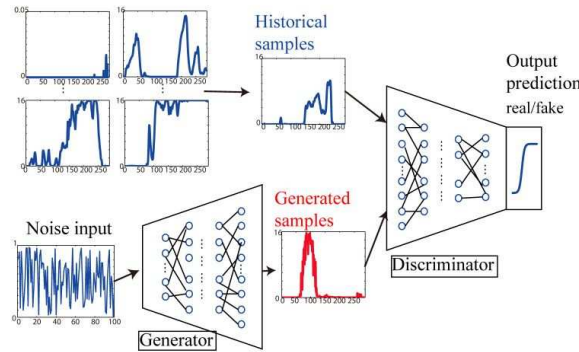


Figure 2.1: Architecture of GANs training procedure, according to Chen et al. [2018]

A GAN training process consists of several iterations where the weights of both neural networks are optimized until the data from the generator is close to the empirical/historical data. This evolution during training can be visualized in case of a two-dimensional data distribution in Figure 2.2. The red data here represents the empirical data to be learned whereas the blue data is generated at the current

stage of training of the generator. One can clearly see that the generated data matches the empirical data more closely when more training iterations of the GAN have taken place.

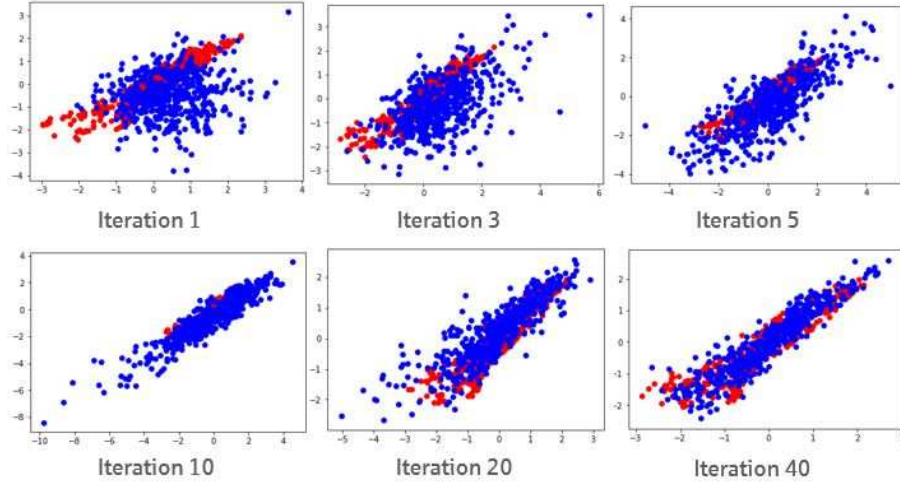


Figure 2.2: Scatterplots of results of a GAN for a two-dimensional data distribution at different training iterations, red = empirical data, blue = generated data

2.3 Application of a GAN as an ESG

The strength of GANs is especially what ESGs should be good at - producing samples of an unknown distribution based on empirical examples of that distribution. Therefore, we will apply a GAN as an ESG.

As shown in Chen et al. [2018], a GAN can be used to create new and distinct scenarios that capture the intrinsic features of the historical data. Fu et al. [2019, p. 3] already noted in their paper that a GAN, as a non-parametric method, can be applied to learn the correlation and volatility structures of the historical time series data and produce unlimited real-like samples that have the same characteristics as the empirical observed time-series. Fu et al. [2019, Chapter 5] have tested this with two stocks and calculated a 1-day VaR.

In our work here, we demonstrate how to expand this to a whole internal model - with enough risk factors to model the full band-width of investments for an insurance company and for a one year time horizon as required in Solvency 2. Diagram 2.3 compares schematically the classical ESG and the idea of a GAN-based ESG and illustrates how this simplifies the classical ESG process.

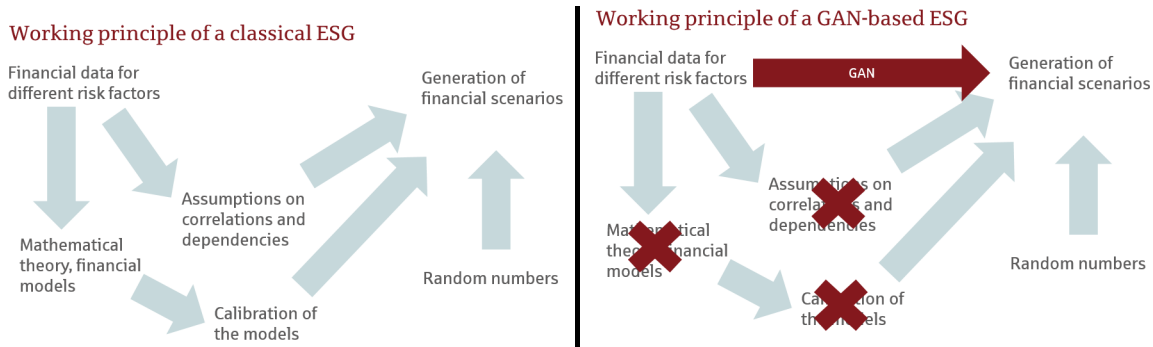


Figure 2.3: Comparison of the working principles of a classical and a GAN-based ESG

The main advantages of a GAN-based ESG, compared to a classical ESG, are:

- *Assumption-free*: A GAN-based ESG can be seen as being assumption-free as it does not contain any financial assumptions regarding distributions of the risk factors and their dependencies. All

information on the risk factors stems directly from the empirically observed data. Assumptions that are enforced by models and that have proven to be wrong afterwards, e.g. the assumption of interest-rates not becoming negative that was popular until the financial crisis 2008/2009, can therefore not lead to a wrong risk assessment.

- *Modeling of dependencies:* As Denuit et al. [2006, Chapter 4] explains, the modeling of dependence structures beyond multivariate normality has become crucial in financial applications. In modern risk models, dependencies are often modeled using copulas. A certain copula has to be selected for each risk-factor and must be fitted so that the desired dependencies are reached. In practice, the modeling of dependencies is very difficult. In a GAN-based model, the dependencies are automatically retrieved from the empirical data.
- *No need for a calibration process:* Calibration of the financial models to match the empirical data is a task that has to be performed regularly by risk managers to keep the models up to date. This is a cumbersome process and there is no standard process for calibration, see DAV (Deutsche Aktuarsvereinigung e.V.) [2015, Chapter 2.1]. This task is not needed for GAN-based models and makes them easier to use. If new data shall be included, the GAN simply has to be fed with the new data.
- *Easy integration of new risk factors:* While the integration of new risk factors in classical ESGs often poses several issues and is quite laborious, in a GAN-based model, expansions of a GAN to include more risk-factors are straightforward.

A disadvantage of a GAN-based ESG is the fact that it purely relies on events that have happened in the past in the financial markets and cannot e.g. produce new dependencies that are not included in the data the model is trained with. Classical financial models aim to derive a theory based on developments in the past and can therefore probably produce scenarios a GAN cannot come up with.

However, it is probable that a GAN-based ESG adapts faster to a regime-switch in one of the risk factors of the model: In a classical ESG a new financial model has to be developed and implemented, whereas a GAN has just to be trained with new data.

3 GAN evaluation measures for GAN-based ESGs

When a GAN is used for scenario generation, the suitability of the generated scenarios of the GAN has to be evaluated, i.e. whether the generated scenarios sufficiently match the empirical observed data. This is important for validation purposes as well as to optimize the GAN infrastructure and the hyperparameters of the two neural networks, the generator and the discriminator.

For example, Figure 3.1 shows the results of the GAN scenario generation after only a few iterations (left) and after a sufficient amount of training iterations (right). The red data in these figures represents the empirical data whereas the blue points represent generated data. GAN evaluation measures should assign a clear and robust value to each scenario generation attempt representing the goodness-of-fit between empirical and generated data. In these cases, the evaluation measure should assign a better value to the scenarios on the right than to those on the left.

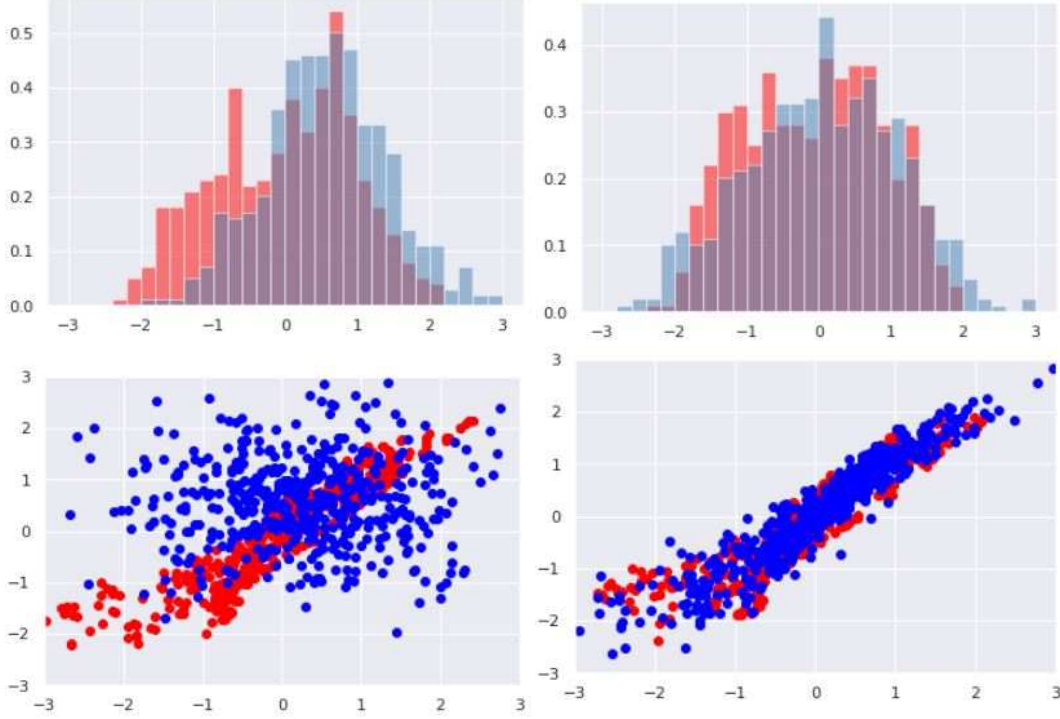


Figure 3.1: Comparison of histograms and scatterplots after a few (left) and after sufficient (right) training iterations, red = empirical data, blue = generated data

In this research, we employ a pure-data driven evaluation approach because one of the main advantages of using a GAN for scenario generation is that no further (financial-mathematical) assumptions on e.g. distributions are necessary and therefore we do not want to use assumptions in the evaluation. Furthermore, we want to take measures that are easily interpretable so they can also be used for validation purposes in Solvency 2.

The suitability of the scenarios can be divided into three categories:

- (1) the alignment between the marginal distributions of empirical observation and generated data for each risk factor
- (2) the alignment of the joint distributions / dependencies between empiric and generated data, i.e. the generated points are near the empirical ones and the GAN does not suffer from “mode collapse”, i.e. all areas of empiric data points are covered by generated data points
- (3) the GAN is not “overfitted” and creates new scenarios instead of memorizing empirical ones.

Measures for these three categories are discussed in Sections 3.1, 3.2 and 3.3, respectively.

For the mathematical discussion in the remainder of this section, we use the following notations:

Let (Ω, \mathcal{F}, P) be a probability space and $d \in \mathbb{N}$ the number of risk factors that we model. In this research, we use a set of $d = 46$ risk factors. The list of those risk factors can be found in Appendix A. $E : \Omega \rightarrow \mathbb{R}^d$ denotes a random vector describing the empirical data, the generated data by a GAN is described by the random vector $G : \Omega \rightarrow \mathbb{R}^d$. Let $m \in \mathbb{N}$ and let E_j , and G_j , $j = 1, \dots, m$, be independent copies of the random vector E and G respectively. Let $\mathbb{E}(\omega) = \{E_1(\omega), \dots, E_m(\omega)\}$ and $\mathbb{G}(\omega) = \{G_1(\omega), \dots, G_m(\omega)\}$ for $\omega \in \Omega$. The target of the GAN is that the generated data G should follow the same (but unknown) distribution as the empirical data E . We denote the distribution functions of E and G by F_E and F_G and the corresponding density functions by f_E and f_G , respectively.

3.1 Measure for the alignment of the distributions: Wasserstein distance

The *Wasserstein distance* is commonly used to calculate the distance between two probability distribution functions, as mentioned in Borji [2019] and Wiese et al. [2020]. We use the univariate Wasserstein

distance to calculate the distance between the marginal distribution functions of E and G for each risk factor. The definition of the Wasserstein distance can be found e.g. in Hallin et al. [2021, p. 5].

In terms of validation, the Wasserstein distance in one dimension can be rewritten as a difference between the quantile functions. Therefore, as Ramdas et al. [2017, Chapter 4.3] states, Wasserstein is a QQ-test which is often used in validation of internal models and therefore fits for our purpose.

3.2 *Measure for the alignment of the dependencies between empiric and generated data: nearest neighbor coincidences*

The test on the alignment of the dependencies of the empiric and generated data can be reformulated as a multivariate two-sample test where we want to measure the equality of two multivariate distributions based on two sets of independent observations. We choose to use the nearest neighbor coincidence measure for this purpose as defined by Schilling [1986] and further developed by Mondal et al. [2015]. This measure serves our purpose as it is easily interpretable: if the dependencies between the empiric data are correctly captured in the generic data set, then half of the nearest neighbors for all data points from each set should belong to the empiric and half to the generated data set.

The measure itself is defined as follows. The indicator function $\mathbf{1}_{E_i}(l)$ takes the value 1 if the l -nearest neighbor (measured in euclidean distance) of data point E_i out of data set $\mathbb{E} \cup \mathbb{G}$ stems from data set \mathbb{E} and zero otherwise. The indicator function $\mathbf{1}_{G_j}(l)$ is defined similarly. Let $k \in \mathbb{N}$. As in Mondal et al. [2015, Chapter 2], we define by

$$T_{1,k} = \frac{1}{mk} \sum_{i=1}^m \sum_{l=1}^k \mathbf{1}_{E_i}(l)$$

the proportion of neighbors of E_i that come from \mathbb{E} and by

$$T_{2,k} = \frac{1}{mk} \sum_{j=1}^m \sum_{l=1}^k \mathbf{1}_{G_j}(l)$$

the proportion of neighbors of G_i that come from \mathbb{G} . A statistic is defined by

$$T_{NN1,k} = \frac{1}{2} |T_{1,k} - \mathbf{E}[T_{1,k}]| + \frac{1}{2} |T_{2,k} - \mathbf{E}[T_{2,k}]|.$$

Mondal et al. [2015] prove that the expectations of $T_{1,k}$ and $T_{2,k}$ satisfy

$$\mathbf{E}[T_{1,k}] = \mathbf{E}[T_{2,k}] = \frac{m-1}{2m-1} \rightarrow \frac{1}{2}, \quad m \rightarrow \infty$$

and that $T_{NN1,k}$ converges to 0 in probability as $m \rightarrow \infty$ if $E_1, \dots, E_m, G_1, \dots, G_m$ are independent and identical distributed and have continuous densities.

3.3 *Measure for the detection of the memorizing effect: memorizing ratio*

Both the Wasserstein distance and the nearest neighbor coincidence statistic will lead to optimal scores if the generated data points exactly match the empirical ones, i.e. $\mathbb{E} = \mathbb{G}$. From a risk management perspective, this is not the optimal result because we want to create new scenarios which could happen instead of memorizing scenarios that have actually taken place, see Chen et al. [2018, p. 2]. Therefore, we need a measure to detect whether the generated data points really differ from the empirical ones and the GAN is not simply memorizing the data points (“overfitting”).

As in a multi-dimensional space it is highly unlikely for generated and empirical data points to match exactly, we classify a generated data point G_j as being memorized if it lays in “an unusual small neighborhood” around an empirical data point. We here define an “unusual small neighborhood” as a fraction $0 < \rho \leq 1$ of the 1-nearest neighbor distance of an empirical data point E_i to the next empirical data point. If a lot of $E_i \in \mathbb{E}$ are closely surrounded by generated data points, then the generated data set is not significantly differing from the empirical one. The memorizing ratio, defined next, describes the proportion of empirical data points where the unwanted memorizing effect occurs.

The next definition is new to literature. The only existing test detecting memorizing in GANs which we found in literature is the birthday paradox test, see Borji [2019]. But this test is based on the visual identification of duplicates for pictures and therefore cannot be utilized in our context.

Definition 1. Let $\rho \in (0, 1]$ and $m \in \mathbb{N}$. The *memorizing ratio* $MR_{\rho, m}$ is defined as:

$$MR_{\rho, m} = \frac{1}{m} \sum_{i=1}^m \mathbf{1}_{[0, \rho R_{E_i}^1)} \left(\min_{j=1, \dots, m} |G_j - E_i| \right) \quad (3.1)$$

where $R_{E_i}^1$ is the distance between E_i and its 1-nearest neighbor out of \mathbb{E} , i.e.

$$R_{E_i}^1 := \min_{i \neq j} |E_i - E_j|, \quad i = 1, \dots, m.$$

A graphical interpretation of the memorizing ratio can be found in Figure 3.2. In this example, E_n is the 1-nearest neighbor of E_i out of the empirical data set \mathbb{E} . The nearest neighbor distance between E_i and E_n is $R := R_{E_i}^1 = |E_n - E_i|$. In Figure 3.2, the data point G_{j_3} counts as a memorized data point whereas G_{j_1} and G_{j_2} are not categorized as being memorized.

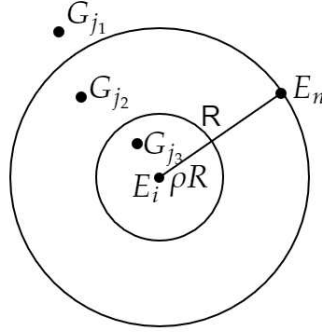


Figure 3.2: Visualization of the definitions in the memorizing ratio context

It is clear that if $\lambda\%$ of the generated data points of \mathbb{G} are simply memorized data points from \mathbb{E} (meaning that $\lambda\%$ of the realizations from \mathbb{G} and \mathbb{E} are (almost) identical), then the expected value of the memorizing ratio is $\mathbf{E}[MR_{\rho, m}] \geq \lambda$. So, we can use this measure to control on the memorizing effect.

Next, we show that the memorizing ratio converges in mean square. We cite the following useful result:

Theorem 2. (Weiss, 1960). Let $E_1, \dots, E_m, G_1, \dots, G_m$ be independent and identically distributed d -variate random variables. Assume E_1 has a piecewise continuous and bounded probability density function f . Let $\rho \in (0, 1]$ and

$$R_i := \rho \min_{i \neq j} |E_i - E_j|, \quad i = 1, \dots, m$$

and let S_i be the number of points G_1, \dots, G_m contained in the open sphere $\{x : |x - E_i| < R_i\}$ for $i = 1, \dots, m$. Then the joint distribution of S_i, S_l is the same as the joint distribution of $S_{i'}, S_{l'}$ for any $i \neq j$ and $i' \neq j'$. It further holds that

$$\lim_{m \rightarrow \infty} P[S_1 = s] = Q(s) := \int_{\mathbb{R}^d} \frac{\rho^{-d} f^{2+s}(x)}{(f(x) + \rho^{-d} f(x))^{s+1}} dx, \quad s \in \mathbb{N}_0 \quad (3.2)$$

and

$$\lim_{m \rightarrow \infty} P[S_1 = s_1 \cap S_2 = s_2] = Q(s_1)Q(s_2), \quad s_1, s_2 \in \mathbb{N}_0.$$

Proof. Lionel Weiss proved the Theorem for $\rho = \frac{1}{2}$ in Weiss [1960] but his proof works exactly the same for any $\rho \in (0, 1]$. \square

Theorem 3. *If the random variables $E_1, \dots, E_m, G_1, \dots, G_m$ are independent and identical distributed and E_1 has a piecewise continuous and bounded probability density function f , the memorizing ratio $MR_{\rho, m}$ converges in mean square to $\frac{\rho^d}{\rho^d + 1}$ for $m \rightarrow \infty$.*

Proof. The proof is based on Theorem 2. It holds

$$\begin{aligned} Q(0) &= \int_{\mathbb{R}^d} \frac{\rho^{-d} f^2(x)}{f(x) + \rho^{-d} f(x)} dx \\ &= \frac{1}{\rho^d + 1} \int_{\mathbb{R}^d} f(x) dx = \frac{1}{\rho^d + 1} < \infty. \end{aligned}$$

Let

$$R_i := \rho \min_{i \neq j} |E_i - E_j| = \rho R_{E_i}^1, \quad i = 1, 2, \dots, m$$

and

$$Z_i := \mathbf{1}_{[0, \rho R_{E_i}^1)} \left(\min_{j=1, \dots, m} |G_j - E_i| \right), \quad i = 1, 2, \dots, m.$$

Then $MR_{\rho, m} = \frac{1}{m} \sum_{i=1}^m Z_i$. It holds by Theorem 2

$$\begin{aligned} \mathbf{E}[Z_i] &= P \left[\min_{j=1, \dots, m} |G_j - E_i| < \rho R_{E_i}^1 \right] \\ &= 1 - P \left[\forall j : |G_j - E_i| \geq R_i \right] \\ &= 1 - P[S_i = 0] \\ &= 1 - P[S_1 = 0] \\ &\rightarrow 1 - Q(0) = \frac{\rho^d}{\rho^d + 1}, \quad i = 1, 2, \dots, \quad m \rightarrow \infty. \end{aligned} \tag{3.3}$$

As $Z_i^2 = Z_i$, it follows

$$\lim_{m \rightarrow \infty} \text{Var}(Z_i) = 1 - Q(0) - (1 - Q(0))^2 = Q(0) - Q^2(0) < \infty, \quad i = 1, 2, \dots$$

Let $i \neq l$. Then

$$\begin{aligned} \text{Cov}(Z_i, Z_l) &= \mathbf{E}[Z_i Z_l] - \mathbf{E}[Z_i] \mathbf{E}[Z_l] \\ &= P \left(\min_{j=1, \dots, m} |G_j - E_i| < \rho R_{E_i}^1 \cap \min_{j=1, \dots, m} |G_j - E_l| < \rho R_{E_l}^1 \right) - (\mathbf{E}[Z_1])^2 \\ &= 1 - P[S_i = 0 \cup S_l = 0] - (E[Z_1])^2 \\ &= 1 - P[S_1 = 0 \cup S_2 = 0] - (E[Z_1])^2 \\ &= 1 - P[S_1 = 0] - P[S_2 = 0] + P[S_1 = 0 \cap S_2 = 0] - (\mathbf{E}[Z_1])^2 \\ &\rightarrow 1 - Q(0) - Q(0) + Q^2(0) - (1 - Q(0))^2 = 0, \quad m \rightarrow \infty. \end{aligned}$$

Hence by Bienaymé's identity

$$\begin{aligned} \mathbf{E} \left[|MR_{\rho, m} - E[Z_1]|^2 \right] &= \text{Var} \left(\frac{1}{m} \sum_{i=1}^m Z_i \right) \\ &= \frac{1}{m^2} \left(\sum_{i=1}^m \text{Var}(Z_i) + \sum_{i \neq l} \text{Cov}(Z_i, Z_l) \right) \\ &= \frac{1}{m^2} (m \text{Var}(Z_1) + (m^2 - m) \text{Cov}(Z_1, Z_2)) \rightarrow 0, \quad m \rightarrow \infty. \end{aligned}$$

Further, by the Minkowski inequality and Equation (3.3), it holds that

$$\begin{aligned} & \sqrt{\mathbf{E} \left[\left| MR_{\rho,m} - \frac{\rho^d}{\rho^d + 1} \right|^2 \right]} \\ & \leq \sqrt{\mathbf{E} \left[|MR_{\rho,m} - E[Z_1]|^2 \right]} + \sqrt{\mathbf{E} \left[\left| E[Z_1] - \frac{\rho^d}{\rho^d + 1} \right|^2 \right]} \rightarrow 0, \quad m \rightarrow \infty. \end{aligned}$$

□

To check for the convergence of the memorizing ratio empirically, we conducted numerical experience for various values of ρ in two different dimensions and with the same distribution for both samples. We conducted this experiment with different distributions (i.e. normal, exponential, student-t, Cauchy, Pareto) and with $m = 500$ data points in each sample and averaged over 10,000 simulations in each case. In Table 1, we compare the results with the theoretical value from Theorem 3.

d	ρ	normal	exponential	student-t	Cauchy	Pareto	theoretical
2	0.1	0.010	0.010	0.011	0.011	0.012	0.010
2	0.3	0.082	0.084	0.084	0.084	0.090	0.083
2	0.5	0.199	0.202	0.199	0.199	0.207	0.200
2	0.7	0.328	0.330	0.326	0.327	0.332	0.329
2	0.9	0.448	0.448	0.445	0.445	0.447	0.448
10	0.1	0.000	0.000	0.000	0.000	0.000	0.000
10	0.3	0.000	0.000	0.005	0.005	0.007	0.000
10	0.5	0.001	0.003	0.022	0.023	0.033	0.001
10	0.7	0.032	0.054	0.086	0.087	0.121	0.027
10	0.9	0.270	0.301	0.309	0.310	0.341	0.259

Table 1: Expectation of the memorizing ratio for $n = 10000$ simulations, $m = 500$ and different values of ρ for the following distributions: standard normal, exponential with mean 1, t-Student with 1 degree of freedom, Cauchy with scale and location equal to 1, Pareto with scale and shape equal to 1.

3.4 Hyperparameter optimization using these evaluation measures

In the preceding sections, we determined a combination of Wasserstein distance for each risk factor $W_i, i = 1, \dots, d$, the nearest neighbor coincidences statistic $T_{NN1,k}$ (abbr. *nnc*) and the memorizing ratio $MR_{\rho,m}$ (abbr. *mr*) being useful to evaluate the quality of the GAN results.

We now want to combine these evaluation measures to optimize the hyperparameters of the two neural networks and the GAN infrastructure itself. In a GAN, a lot of different variants can be tested. A full optimization is not possible as, see Motwani and Parmar [2020, Chapter 2], the “selection of the GAN model for a particular application is a combinatorial exploding problem with a number of possible choices and their orderings. It is computationally impossible for researchers to explore the entire space.” So, in our work, we check on the following sequentially:

- Number of layers for generator and discriminator: Not only the number itself, but also the relation between the number of layers in each neural network can make a big difference.
- Number of neurons per layer: This, too, can be different between the two neural networks and can also vary from layer to layer inside a network.
- Dimension of the latent space: The latent space where the input for the generator is sampled usually has a higher dimensionality than the dimension of the generator’s output.

- Number of training iterations of the generator versus discriminator: The generator is usually trained n times in each iteration while the discriminator is trained once. We will check for an optimal parameter n .
- Functions used in the GAN: The activation functions in the layers of the two networks, the optimization algorithm and the usage of batch normalization can be varied.

We performed our experiments for $d = 46$ dimensions and with the parameters for nnc and mr of $k = 3$ and $\rho = 0.5$. The risk factors used are derived from the MCRCS study conducted by EIOPA (see EIOPA MCRCS Project Group [2020b]) and will be further discussed in Section 4.

Figure 3.3 shows the development of the Wasserstein distances for all 46 risk factors and the development of the other two measures with both neural networks having 4 layers over the 2500 training iterations:

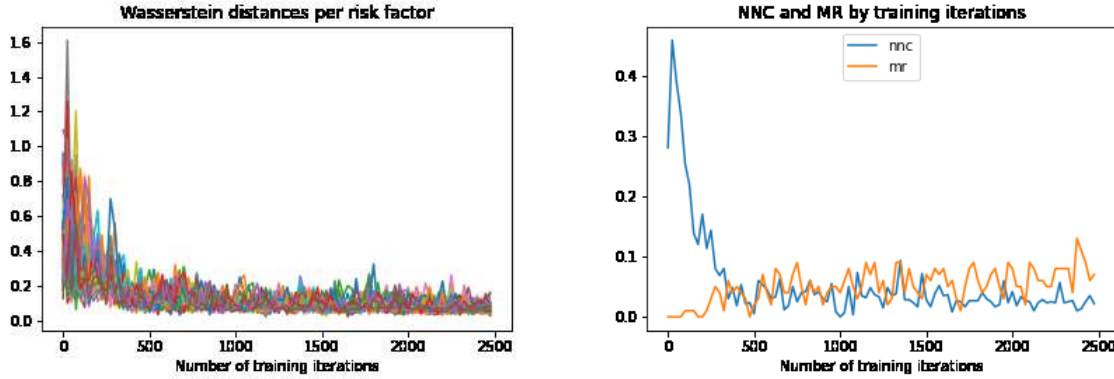


Figure 3.3: Development of the chosen GAN evaluation measures for a GAN

In the left panel of Figure 3.3, we can see that the Wasserstein distances of all risk factors converge with increasing training iterations. In the right figure, one can clearly see the behavior of the memorizing ratio serving as an opponent to the nearest neighbor coincidences measure: Over the training iterations, the data distributions get closer and closer, and therefore the nnc measure decreases near to its expected value 0.

The expected value of the memorizing ratio in this case is close to zero ($\frac{0.5^{46}}{0.5^{46}+1} \approx 10^{-14}$), see Theorem 3. The memorizing ratio, however, increases with more training iterations. As explained above, a large number of memorized points is undesirable. Therefore, the omission of this ratio would lead to the selection of a non-optimal GAN architecture for this application as one would train the GAN longer leading to overfitting.

Next, we aggregate the values from the measures in each evaluation run and define the following *target function*

$$tf = \frac{1}{3} \left(\max_{i=1, \dots, 46} (W_i) + T_{NN1,k} + \left| MR_{\rho,m} - \frac{\rho^d}{\rho^d + 1} \right| \right)$$

Our experience shows that simply taking the average of the three measures works well. In other contexts, it can make sense to introduce some kind of weighting in this formula.

The measures for the differences between joint distributions nnc and mr can be evaluated in a space with the same dimension as the input parameters, so one figure per measure is obtained. For mr , we subtract the limiting value for $m \rightarrow \infty$ under the assumptions of Theorem 3. The Wasserstein distance, however, is determined for each risk factor, in our case leading to 46 figures. To aggregate, we use the maximum over these 46 risk factors, which leads to one figure for the Wasserstein distance, too.

Figure 3.4 demonstrates the development of the tf -value over the training iterations for a configuration with both neural networks having 4 layers. As it is computationally expensive to calculate this tf -value in every iteration of the GAN training, we decide to determine the tf -value every 25

training iterations where 25 is a compromise between accuracy and computational feasibility.

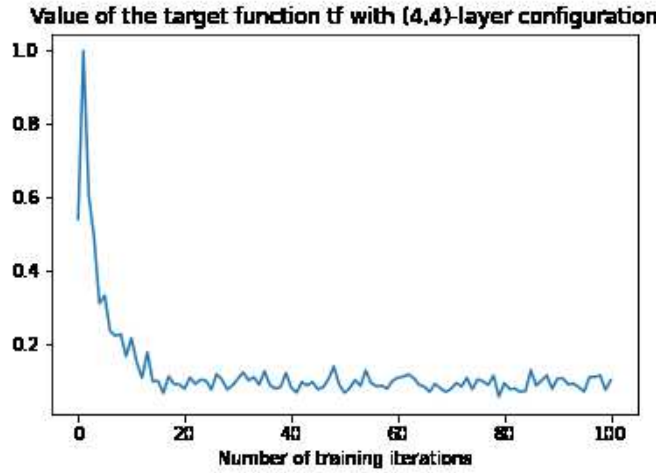


Figure 3.4: Development of the tf -value for a GAN

Based on the tf -value, one can then select not only the best architecture, but also the optimal number of training iterations. In the experiments, one can clearly see that the GAN is not converging but there is a minimum of the target function during training and afterwards the tf -value starts increasing again. This is the behaviour typically seen in GAN training, see e.g. Goodfellow [2016, p. 34].

As a next step, we want to show which parameters have significant influence on the outcome and how a optimization can be performed. We will use a step-wise approach where we first check on the sensitivities according to the number of layers, and find the best configuration there and then take these results as a basis for the next check.

First, we run the GAN with 16 different configurations of layers for the discriminator D and the generator G. For each neural network we use between 2 and 8 layers in steps of 2 layers. The resulting tf -values are the following (the number of layer in D are in the rows, those of G in the columns):

number of layers in D/G	2	4	6	8
2	0.061	0.446	0.479	0.423
4	0.097	0.058	0.084	0.082
6	0.325	0.091	0.077	0.077
8	0.356	0.214	0.119	0.083

Table 2: tf -values for varying number of layers in both networks

The minimum of our target function tf is reached for both neural networks having 4 layers (marked in bold). We cannot confirm in this experiment the thesis of Goodfellow [2016, p. 33], which states that the discriminator is usually deeper than the generator. What we can clearly see is that the number of layers plays an important role in the performance of the GAN.

The number of inputs at the input layer of the generator equals the dimension of the latent space. The output layer of the generator has exactly 46 neurons, each being the value for one risk factor. The discriminator has a input layer with 46 neurons and an one-dimensional output. So, we can vary the two layers in between and the dimension of the latent space. First, we run the GAN with 12 different configurations of neurons per layer for the discriminator D and the generator G. In this experiment, we always set the number of neurons per layer being equal inside the respective neural network. The

resulting tf -values are the following (the number of neurons per layer in D are in the rows, those of G in the columns):

number of neurons per layer in D/G	100	200	400
100	0.072	0.083	0.083
200	0.055	0.058	0.060
400	0.048	0.044	0.058
600	0.056	0.054	0.055

Table 3: tf -values for varying number of neurons per layer in both networks

The differences between the different configurations in this case are less pronounced than for the experiment with different numbers of layers before. So, we can state that the optimization of the number of layers is more important than the choice of the number of neurons per layer. The minimum of our target function tf is reached for the discriminator having 400 and the generator having 200 neurons per layer (marked in bold).

Now, we want to vary the dimension of the latent space to check whether this improves the performance further. The dimension of the latent space in the (400,200)-neurons configuration was 200. To check sensitivity on the dimension for the latent space, we now check the same configuration with 100 and 400 as dimensions of the latent space. The following table shows the values of the target function tf for different dimensions:

dimension of latent space	100	200	400
value of tf	0.055	0.044	0.063

Table 4: tf -values for varying dimension of the latent space in the generator network

The results show that the sensitivity to the dimension of the latent space is similar to the sensitivity to the number of neurons per layer. The value of 200 seems to be optimal in this case, so the dimension of the latent space equals the number of neurons per layer in the generator.

In practice of a GAN training, the training alternates between n steps of optimizing the generator G and one step of optimizing the discriminator D . Now, we will examine whether n has a significant impact on the performance of our GAN and what a good value in our application is. Our experiments with 7 different values of the iteration parameter n lead to the following results:

n	1	3	5	8	10	12	15
value of tf	0.057	0.057	0.057	0.053	0.044	0.062	0.054

Table 5: tf -values for varying number of trainings for G in each training iteration for D

So, our experiments show that it is indeed advisable to train the generator more often than the discriminator. In our case, a value of 10 seems to be appropriate. However, this seems to be a parameter which is not very important for the performance of the GAN as many parameters n show a similar value of tf .

For the optimization of GAN architecture, we first want to examine which optimizer to use. The use of the Adam optimizer rather than SGD is proposed by Goodfellow [2016] and Lucic et al. [2017]. We try with three different optimizers (Adam, SGD and RMSprop) and get the following results:

optimizer	Adam	SGD	RMSprop
value of tf	0.044	0.057	0.077

Table 6: tf -values for different optimisers

As proposed in literature, the optimizer Adam seems to lead to the best result whereas RMSprop leads to the worst result. We will therefore stick to optimizer Adam.

In the last optimization step, we want to examine the usefulness of the batch normalization. Radford et al. [2015, p. 3] states that this stabilizes the training process and prevents mode collapse. So, we tried one GAN with batch normalization between the layers and one without batch normalization:

batch normalization	yes	no
value of tf	0.044	0.436

Table 7: tf -values for a GAN with and without batch normalization

The GAN model without batch normalization does not converge at all which is reflected at the very high value of tf . Batch normalization therefore seems to be crucial for our GAN model to work.

Based on our analysis of these different settings for the number of layers, the number of neurons, the training iterations, the dimensions of the latent space and inner functions, we found the following configuration for our GAN-based ESG leading to best results:

- 4 layers for discriminator and generator
- 400 neurons per layer in the discriminator and 200 in the generator
- 10 training iterations for the generator in each discriminator training
- Dimension of the latent space is 200
- We use LeakyReLU as activation functions, except for the output layers which use Sigmoid (for discriminator) and linear (for generator) activation functions. We use the Adam optimizer and batch normalization after each of the layers in the network.

We use the trained generator with this configuration at a sufficient number of training iterations to generate the scenarios for our comparison with the results of classical ESGs in the next section.

4 Comparison of GAN results with the results of the MCRCS study

4.1 Introduction to the MCRCS study

Since 2017, the EIOPA (European Insurance and Occupational Pensions Authority) performs an annual study, called the *market and credit risk comparison study*, abbr. MCRCS. According to the instructions from EIOPA MCRCS Project Group [2020b], the "primary objective of the MCRCS is to compare market and credit risk model outputs for a set of realistic asset portfolios". In the study, all insurance undertakings with significant exposure in EUR and with an approved internal model are asked to participate, see EIOPA [2021]. In the study as of year-end 2019, 21 insurance companies from 8 different countries of the European Union participated.

All participants have to model the risk of 104 different synthetic instruments. Those comprise all relevant asset classes, i.e. risk-free interest rates, sovereign bonds, corporate bonds, equity indices, property, foreign exchange and some derivatives. A detailed overview of the synthetic instruments that are used in this study can be found in EIOPA MCRCS Project Group [2020a].

Additionally, those instruments are grouped into 10 different asset-only benchmark portfolios, 2 liability-only benchmark portfolios and 10 combined portfolios. These portfolios "should reflect typical asset risk profiles of European insurance undertakings", see EIOPA MCRCS Project Group [2020b, Section 2]. This analysis sheds light into the interaction and dependencies between the risk factors. Figure 4.1 presents the asset-type composition of the asset-only benchmark portfolios.

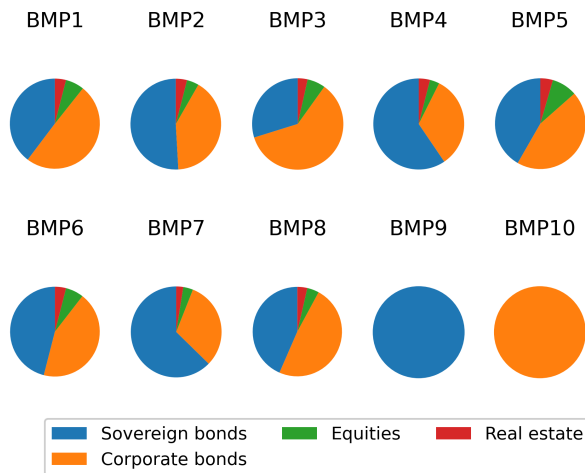


Figure 4.1: Composition of the MCRCS asset-only benchmark portfolios BMP1 - BMP10

All asset portfolios mainly consist of fixed income securities (86% to 94%) as this forms the main investment focus of insurance companies. However, there are significant differences both in ratings, durations and also in the weighting between sovereign and corporate exposures. The two liability profiles are assumed to be zero-bond based, so they represent the liabilities of non-life insurance companies and differ in their durations (13.1 years vs. 4.6 years). The combined portfolios are linear combinations of these asset and liability benchmark portfolios.

4.2 Methodology and data

For the purpose of this article, we will only compare the risk charges for instruments that are also included in the benchmark portfolios. An aggregated view of these instruments together with the used Bloomberg sources can be found in Appendix A. As the study used here is at year-end 2019, we take the datapool from end of March 2002 until Dec. 2019 as the basis of our GAN training. We therefore have 4587 daily observations in this dataset which comprises almost 18 years including the financial crisis 2008/2009.

In Solvency 2, we have to model the market risk for a one year time horizon. There are two approaches to derive the risk based on higher frequent data (here daily returns) for a longer horizon (here annually). One solution, see Fu et al. [2019], is to use the daily data to train the GAN model and then use some autocorrelation function to generate an annual time series based on daily returns. The other solution is to use overlapping rolling windows of annual returns on a daily basis for the training of the model. We use in this work overlapping rolling windows as explained in Wiese et al. [2020, p. 16] and EIOPA [2021, p. 17].

Annually, EIOPA publishes a detailed study with an anonymized comparison of the risk charges of the different insurance companies' market risk models by portfolios, instruments and some additional analysis, e.g. dependencies of the risk factors. The study for year-end 2019 can be found on the EIOPA homepage, see EIOPA [2021].

4.3 Comparison on risk-factor level

The results on risk factor basis are analyzed based on the shocks generated or implied by the ESGs. A shock hereby is defined in EIOPA [2021, p. 11] as

Definition 4. A *shock* is the absolute change of a risk factor over a one-year time horizon. Depending on the type of risk factor, the shocks can either be two-sided (e.g. interest rates 'up/down') or one-sided (e.g. credit spreads 'up'). This metric takes into account the undertakings' individual risk measure definitions and is based on the 0.5% and 99.5% quantiles for two-sided risk factors and the 99.5% quantile for one-sided risk factors, respectively.

The results are presented in diagrams, showing boxes with whiskers for each maturity / sub-type of the risk factors. The boxes contain the shocks of the participating insurance companies between the 25% and 75% percentile of all participants. The whiskers extend this to the 10% and 90% percentile. The sample consists of 21 participants at maximum; results are only provided if an insurance company states at least some exposure to this risk factor.

We enrich those results with a blue dot representing the shock for that risk factor generated by our GAN-based model. In this work, we will show the comparison of the four most important risk factor categories (corporate credit spread, equity, interest rate up and down). Other risk factors show a similar behaviour.

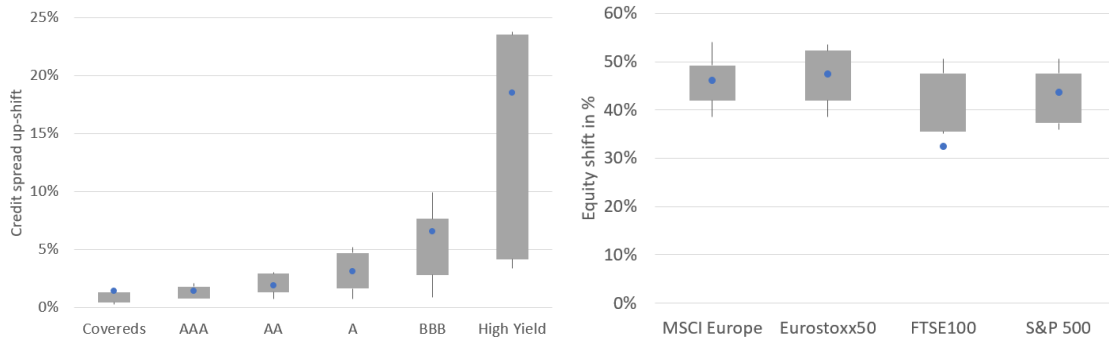


Figure 4.2: Comparison of the simulated shifts for the credit spread and equity risk factors, representation based on own results and EIOPA [2021, p. 25 and 27]

For credit spreads in Figure 4.2, we see a very good alignment between the GAN-based model and the approved internal models. On the equity side, the shifts are also similar for most of the risk factors. For the FTSE100, the GAN produces less severe shocks than the other models. This behaviour, however, can actually be found in the training data as the FTSE100 is less volatile than the other indices for the time frame used in GAN training. So, the GAN here produces plausible results.

For interest rates, however, the picture is more complex as Figure 4.3 illustrates:

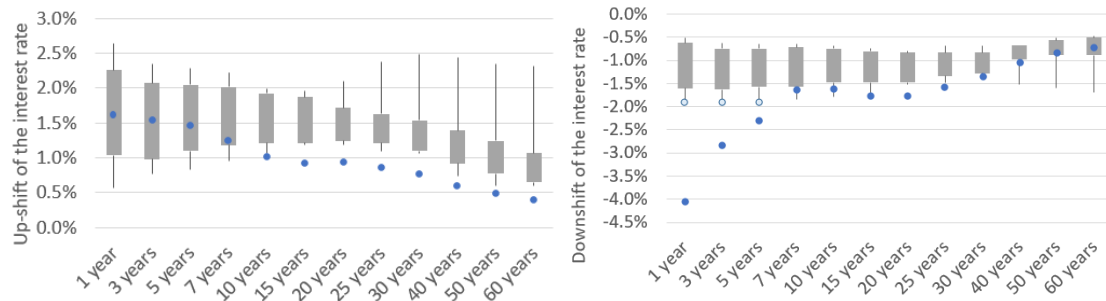


Figure 4.3: Comparison of the simulated shifts (left: up, right: down) for the interest rate risk factors, representation based on own results and EIOPA [2021, p. 22]

The up-shifts generated by the GAN-based model are within the boxes for 1 to 7 year buckets. Afterwards, the shifts are below the whiskers. This effect is due to the time span of the data used for the training of the GAN. The interest rates in this time period (Mar. 2002 - Dec. 2019) are mostly decreasing. In the traditional ESGs, the interest rates are probably calibrated on a longer horizon

so they include upward trends in long term interest rates from a longer history. However, since the availability of consistent market data gets more difficult if one goes further back in history, we use the time horizon since 2002 in our GAN training. If an insurance company wants to include more up-shifts in the training, the training data has to be transformed accordingly. This, however, would deviate from the idea of the GAN-based ESG as a full data-driven model. Additionally, it is a valid point to discuss whether the interest rate movements having occurred in a different regime with much higher interest rates are meaningful for the fluctuations in a current low interest rate environment.

For the down-shifts, the graph shows a contrary behaviour: The short- and medium term interest rates are far below the whiskers, whereas the longer term interest rates mostly are inside the whiskers or boxes. This also can be explained by the interest rate development: The time span used for training of the GAN shows a sharp decrease of interest rates especially in the short term whereas longer term interest rates behaved more stable. This behaviour is mimicked by the GAN. In traditional ESGs, additionally to the longer time span used for calibration, often expert judgement by the insurers leads to a lower bound on how negative interest rates can become. One of the most common arguments for a lower bound of interest rates according to Grasselli and Lipton [2019, Chapter 4] is the fact that instead of investing money with negative interest rates, asset managers could also convert the money into cash and store this. However, the conversion of large amounts of money into cash poses a lot of issues and is therefore unrealistic. Grasselli and Lipton [2019] derive a cash-related physical lower bound of about -0.5% with this argument. Danthine [2017, Chapter 2] states that the lower boundary for interest rates is not far below -0.75% in current environment. For illustration purposes, we introduced light blue dots in Figure 4.3 where we limited the downshift to -1.9% in the GAN (as this is the value of the lower whisker). This, however, didn't change the results on the portfolio level as presented in Section 4.4 significantly (difference in VaR always below 0.1%). We didn't pursue this approach further as we want to stick with a pure data-driven model but this would be a reasonable approach if an insurance company wants to limit downside interest rate shifts.

4.4 Comparison on portfolio level

The main comparison between the results for the benchmark portfolios is based on the risk charge which is defined in EIOPA MCRCS Project Group [2020b, Section 2].

Definition 5. The *risk charge* is the ratio of the modeled Value at Risk (99.5%, one year horizon) and the provided market value of the portfolio.

In this work, we only show the comparison of the risk charges for the combined asset-and-liabilities portfolios. The comparisons for asset-only and liability-only benchmark portfolios follow a similar pattern.

Figure 4.4 displays the risk charge for each of the benchmark portfolios which comprises portfolios with the longer (left) and the shorter liability structure (right). As in the comparison for the risk factors, the gray boxes contain the risk charges of the participating insurance companies between the 25% and 75% percentile. The whiskers extend this to the 10% and 90% percentile. The sample consists of 21 participants, so 4 results (2 above, 2 below the whiskers) are not shown. The risk charge according to our GAN-based model is represented by a blue dot.

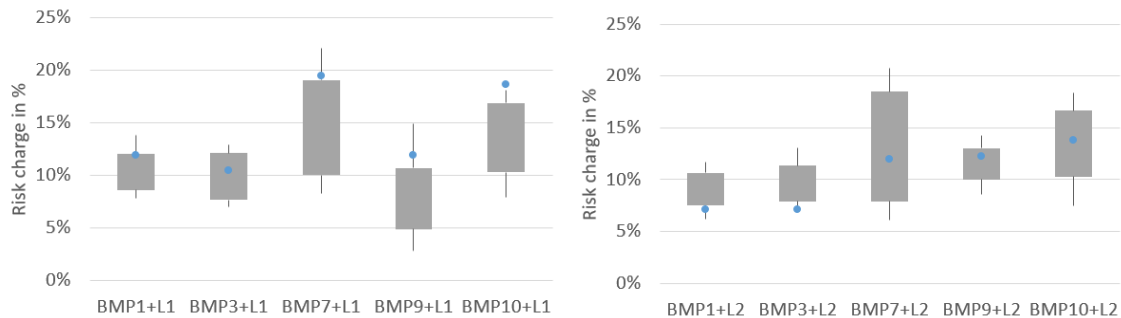


Figure 4.4: Comparison of the combined asset-liability benchmark portfolios, representation based on own results and EIOPA [2021, p. 14]

The risk charge of the GAN-based model fits well to the risk charges of the established models. On the left side (longer liability structure), the blue dot always is in the upper percentile of the risk charges or slightly above the 90%-percentile. Due to the duration profile of this portfolio, the risk charge is generated by scenarios with decreasing interest rates. In the risk factor comparison of the interest rate down shock, the interest rate down shifts are more severe in most maturities for the GAN-based model than for the classical models. Therefore, it seems plausible for the resulting portfolio risk to be at the upper percentiles, too.

The right graph (shorter liability structure) shows a different picture: The risk charge of the GAN-based model mostly lies within the boxes or within the lower whiskers. This is due to the fact that for this portfolio structure, increasing interest rates form a main risk. As the shocks for the GAN-based model for increasing interest rates are within the boxes or even below the boxes, this behaviour can be explained, too.

Overall, the resulting risk charges for the GAN-based model are comparable to the results of the approved internal models in Europe. Therefore, GAN-based models can be seen as an appropriate alternative way of market risk modeling.

5 Summary and Conclusion

In this research, we have shown how a generative adversarial network (GAN) can serve as an economic scenario generator (ESG) for the calculation of market risk in insurance companies. Compared to the current approaches, a GAN-based ESG is an assumption-free approach that can model complex dependencies between risk factors appropriately.

For validation purposes as well as for the optimization of the GAN itself, we provided three measures that can evaluate the performance of the scenario generation of the GAN: Wasserstein distance (measuring the alignment of the distributions of the risk factors), nearest neighbor coincidences (measuring the alignment of the dependencies between the risk factors) and a new measure, the memorizing ratio (measuring overfitting). We provided a framework how these measures can be used in the hyperparameter and GAN architecture optimization process.

Finally, we showed that the results of a GAN-based ESG are comparable to the currently used ESGs when using the EIOPA MCRCs study as a benchmark. Therefore, GAN-based ESGs can be an useful alternative way of market risk modeling.

Note. The authors declare that they have no conflict of interest.

Acknowledgement. S. Flaig would like to thank Deutsche Rückversicherung AG for the funding of this research. Opinions, errors and omissions are solely those of the authors and do not represent those of Deutsche Rückversicherung AG or its affiliates.

References

- Alankrita Aggarwal, Mamta Mittal, and Gopi Battineni. Generative adversarial network: An overview of theory and applications. *International Journal of Information Management Data Insights*, page 100004, 2021.
- Christoph Bennemann. *Handbuch Solvency II: von der Standardformel zum internen Modell, vom Governance-System zu den MaRisk VA*. Schäffer-Poeschel, 2011.
- Peter J Bickel and Leo Breiman. Sums of functions of nearest neighbor distances, moment bounds, limit theorems and a goodness of fit test. *The Annals of Probability*, pages 185–214, 1983.
- Ali Borji. Pros and cons of gan evaluation measures. *Computer Vision and Image Understanding*, 179: 41–65, 2019.
- Yize Chen, Pan Li, and Baosen Zhang. Bayesian renewables scenario generation via deep generative networks. In *2018 52nd Annual Conference on Information Sciences and Systems (CISS)*, pages 1–6. IEEE, 2018.

- Francois Chollet. *Deep learning with Python*. Manning, 2018.
- Jean-Pierre Danthine. The interest rate unbound? *Comparative Economic Studies*, 59(2):129–148, 2017.
- DAV (Deutsche Aktuarsvereinigung e.V.). Zwischenbericht zur Kalibrierung und Validierung spezieller ESG unter Solvency II. Ergebnisbericht des Ausschusses Investment der Deutschen Aktuarvereinigung e.V., 2015. URL https://aktuar.de/unsere-themen/fachgrundsaeetze-oeffentlich/2015-11-09_DAV-Ergebnisbericht_Kalibri
- Michel Denuit, Jan Dhaene, Marc Goovaerts, and Rob Kaas. *Actuarial theory for dependent risks: measures, orders and models*. John Wiley & Sons, 2006.
- Bruno Ebner, Norbert Henze, and Joseph E Yukich. Multivariate goodness-of-fit on flat and curved spaces via nearest neighbor distances. *Journal of Multivariate Analysis*, 165:231–242, 2018.
- Florian Eckerli and Joerg Osterrieder. Generative adversarial networks in finance: an overview. *arXiv preprint arXiv:2106.06364*, 2021.
- EIOPA. The underlying assumptions in the standard formula for the solvency capital requirement calculation, 2014. URL https://www.bafin.de/SharedDocs/Downloads/EN/Leitfaden/VA/dl_lf_solvency_annahmen_standardformel_sc
- EIOPA. 2018 EIOPA Insurance Stress Test report, 2018. URL https://www.eiopa.europa.eu/sites/default/files/eiopa_2018_insurance_stress_test_report.pdf.
- EIOPA. YE2019 Comparative Study on Market & Credit Risk Modelling, 2021. URL <https://www.eiopa.europa.eu/sites/default/files/publications/reports/2021-study-on-modelling-of-ma>
- EIOPA MCRCS Project Group. Specification of financial instruments and benchmark portfolios of the Year-end 2019 edition of the Market and credit risk modelling comparative study, 2020a. URL https://www.eiopa.europa.eu/sites/default/files/toolsanddata/mcrs_2019_instruments_and_bmp.xlsx.
- EIOPA MCRCS Project Group. Market & credit risk modelling comparative study (MCRCS), year-end 2019 edition: Instructions to participating undertakings for filling out the data request, 2020b. URL https://www.eiopa.europa.eu/sites/default/files/toolsanddata/mcrs_year-end_2019_instructions_covid
- European Commission. Commission delegated regulation (EU) 2015/35 of 10 October 2014 supplementing directive 2009/138/EC of the European parliament and of the council on the taking-up and pursuit of the business of insurance and reinsurance (Solvency II). *Official Journal of European Union*, 2015.
- Rao Fu, Jie Chen, Shutian Zeng, Yiping Zhuang, and Agus Sudjianto. Time series simulation by conditional generative adversarial net. *arXiv preprint arXiv:1904.11419*, 2019.
- Ian Goodfellow. Nips 2016 tutorial: Generative adversarial networks. *arXiv preprint arXiv:1701.00160*, 2016.
- Ian Goodfellow, J. Pouget-Abadie, and M. et al Mirza. Generative adversarial nets. *Advances in neural information processing systems*, 2014.
- Matheus R Grasselli and Alexander Lipton. On the normality of negative interest rates. *Review of Keynesian Economics*, 7(2):201–219, 2019.
- Helmut Gründl, Mirko Kraft, Thomas Post, Roman N Schulze, Sabine Pelzer, and Sebastian Schlütter. *Solvency II-Eine Einführung: Grundlagen der neuen Versicherungsaufsicht*. VVW GmbH, 2nd edition, 2019.
- Marc Hallin, Gilles Mordant, and Johan Segers. Multivariate goodness-of-fit tests based on wasserstein distance. *Electronic Journal of Statistics*, 15(1):1328–1371, 2021.
- Pierre Henry-Labordere. Generative models for financial data. *Available at SSRN 3408007*, 2019.

- Norbert Henze. A multivariate two-sample test based on the number of nearest neighbor type coincidences. *The Annals of Statistics*, 16(2):772–783, 1988.
- Edmond Lezmi, Jules Roche, Thierry Roncalli, and Jiali Xu. Improving the robustness of trading strategy backtesting with boltzmann machines and generative adversarial networks. *Available at SSRN 3645473*, 2020.
- Ziqiang Li, Rentuo Tao, and Bin Li. Regularization and normalization for generative adversarial networks: A review. *arXiv preprint arXiv:2008.08930*, 2020.
- Mario Lucic, Karol Kurach, Marcin Michalski, Sylvain Gelly, and Olivier Bousquet. Are gans created equal? a large-scale study. *arXiv preprint arXiv:1711.10337*, 2017.
- Pronoy K Mondal, Munmun Biswas, and Anil K Ghosh. On high dimensional two-sample tests based on nearest neighbors. *Journal of Multivariate Analysis*, 141:168–178, 2015.
- Tanya Motwani and Manojkumar Parmar. A novel framework for selection of GANs for an application. *arXiv preprint arXiv:2002.08641*, 2020.
- Hao Ni, Lukasz Szpruch, Magnus Wiese, Shujian Liao, and Baoren Xiao. Conditional sig-wasserstein gans for time series generation. *arXiv preprint arXiv:2006.05421*, 2020.
- Dietmar Pfeifer and Olena Ragulina. Generating VaR scenarios under Solvency II with product beta distributions. *Risks*, 6(4):122, 2018.
- Alec Radford, Luke Metz, and Soumith Chintala. Unsupervised representation learning with deep convolutional generative adversarial networks. *arXiv preprint arXiv:1511.06434*, 2015.
- Aaditya Ramdas, Nicolás García Trillos, and Marco Cuturi. On wasserstein two-sample testing and related families of nonparametric tests. *Entropy*, 19(2):47, 2017.
- Mark F Schilling. Multivariate two-sample tests based on nearest neighbors. *Journal of the American Statistical Association*, 81(395):799–806, 1986.
- Lionel Weiss. Two-sample tests for multivariate distributions. *The Annals of Mathematical Statistics*, 31(1):159–164, 1960.
- Magnus Wiese, Lianjun Bai, Ben Wood, and Hans Buehler. Deep hedging: learning to simulate equity option markets. *arXiv preprint arXiv:1911.01700*, 2019.
- Magnus Wiese, Robert Knobloch, Ralf Korn, and Peter Kretschmer. Quant gans: Deep generation of financial time series. *Quantitative Finance*, 20(9):1419–1440, 2020.

Appendix

A Table of instruments used for the MCRCS study

Here is the ticker list from Bloomberg for the data used for the market risk scenario generation:

Asset Class	Subtype	Maturity	Bloomberg ticker
Government bond	Austria	5, 10 years	GTATS5Y/10Y Govt
	Belgium	5, 10 years	GTBEF5Y/10Y Govt
	Germany	5, 10 years	GTDEM5Y/10Y Govt
	Spain	5, 10 years	GTESP5Y/10Y Govt
	France	5, 10 years	GTFRF5Y/10Y Govt
	Ireland	5, 10 years	GIGB5Y/10Y Index

Asset Class	Subtype	Maturity	Bloomberg ticker
	Italy	5, 10 years	GTITL5Y/10Y Govt
	Netherlands	5, 10 years	GTNLG5Y/10Y Govt
	Portugal	5 years	GSPT5YR Index
	UK	5 years	C1105Y Index
	US	5 years	H15T5Y Index
Covered bond	issued by AA-rated bank	5, 10 years	C9235Y/C92310Y Index
Corporate bond	senior unsecured bond, rating AA	5, 10 years	C6675Y/C66710Y Index
	senior unsecured bond, rating A	5, 10 years	C6705Y/C67010Y Index
	senior unsecured bond, rating BBB	5, 10 years	C6735Y/C67310Y Index
Interest rates	EUR, risk-free	1 - 50 years	S0045Z 1Y/.../50Y BLC2 Curncy
	USD, risk-free	5 years	USSW5 Index
	GBP, risk-free	5 years	BPSW5 Index
Equity	EuroStoxx50	-	SX5T Index
	MSCI Europe	-	MSDEE15N Index
	FTSE100	-	TUKXG Index
	S&P500	-	SPTR500N Index
Real-estate	Europe, commercial	-	EXUK Index

This figure "17N__Gemeinsam_Marktrisiko_Flaig_DataScientist____sdateien_Bilde

<http://arxiv.org/ps/2109.10072v2>

This figure "18N__Gemeinsam_Marktrisiko_Flaig_DataScientist____sdateien_Bilde

<http://arxiv.org/ps/2109.10072v2>

This figure "13N__Gemeinsam_Marktrisiko_Flaig_DataScientist____tionsdateien_B

<http://arxiv.org/ps/2109.10072v2>

This figure "14N__Gemeinsam_Marktrisiko_Flaig_DataScientist____tionsdateien_B

<http://arxiv.org/ps/2109.10072v2>

This figure "15N__Gemeinsam_Marktrisiko_Flaig_DataScientist____nsdateien_Bild

<http://arxiv.org/ps/2109.10072v2>

This figure "16N__Gemeinsam_Marktrisiko_Flaig_DataScientist____rLyx_4_3_Ve

<http://arxiv.org/ps/2109.10072v2>

This figure "0N__Gemeinsam_Marktrisiko_Flaig_DataScientist_P____rLyx_GAN_A

<http://arxiv.org/ps/2109.10072v2>

This figure "10N__Gemeinsam_Marktrisiko_Flaig_DataScientist____omotionsdateie

<http://arxiv.org/ps/2109.10072v2>

This figure "11N__Gemeinsam_Marktrisiko_Flaig_DataScientist____n_Promotionsd

<http://arxiv.org/ps/2109.10072v2>

This figure "12N__Gemeinsam_Marktrisiko_Flaig_DataScientist____on_Promotions

<http://arxiv.org/ps/2109.10072v2>

This figure "1N__Gemeinsam_Marktrisiko_Flaig_DataScientist_P____teien_BilderF_

<http://arxiv.org/ps/2109.10072v2>

This figure "2N__Gemeinsam_Marktrisiko_Flaig_DataScientist_P____ien_BilderF__r

<http://arxiv.org/ps/2109.10072v2>

This figure "3N__Gemeinsam_Marktrisiko_Flaig_DataScientist_P____nsdateien_Bild

<http://arxiv.org/ps/2109.10072v2>

This figure "4N__Gemeinsam_Marktrisiko_Flaig_DataScientist_P____Histogramm_E

<http://arxiv.org/ps/2109.10072v2>

This figure "5N__Gemeinsam_Marktrisiko_Flaig_DataScientist_P____Histogramm_E

<http://arxiv.org/ps/2109.10072v2>

This figure "6N__Gemeinsam_Marktrisiko_Flaig_DataScientist_P__catterplot_Beis

<http://arxiv.org/ps/2109.10072v2>

This figure "7N__Gemeinsam_Marktrisiko_Flaig_DataScientist_P__catterplot_Beis

<http://arxiv.org/ps/2109.10072v2>

This figure "8N__Gemeinsam_Marktrisiko_Flaig_DataScientist_P__tionsdateien_B

<http://arxiv.org/ps/2109.10072v2>

This figure "9N__Gemeinsam_Marktrisiko_Flaig_DataScientist_P____lderF__rLyx_d

<http://arxiv.org/ps/2109.10072v2>